Cryptic Magma Chamber in the Deccan Traps imaged using receiver function

Gokul Saha, Vivek Kumar, Dipak K. Chaubey, and Shyam S. Rai

Department of Earth and Climate Science,
Indian Institute of Science Education & Research Pune,
Dr. Homi Bhabha Road, Pune-411008, India

Corresponding author: kumarsahagokul123@gmail.com

Key Points:

- First quantitative constraint on the magma plumbing system in the Deccan Volcanic Province, India.
- Frozen magma chamber at 8-17 km depth seismically imaged as a low-velocity layer.
- 10-15 km thick magma underplating beneath the west coast of the Deccan traps.

Abstract

We present the first evidence for a lower S-wave velocity (Vs ~3.3 to 3.5 km/s) at 8-17 km depth underlying a 4 km thick high-velocity zone with Vs >3.8 km/s beneath the west coast and the neighbouring parts of the Deccan Volcanic Province, India, coinciding with the last phase of volcanism. The velocity structure is derived from joint inversion of receiver function from 9 seismographs operated along ~106 km long W-E profile with the surface wave dispersion data. The low-velocity layer possibly represents the horizontally elongated frozen magma reservoir, the source for the magma eruption at ~65 million years produced due to the interaction of the Reunion hotspot with India. The shallow, high-velocity layer could be basaltic mafic intrusions responsible for the production of massive CO_2 degassing. The Moho deepens beneath the west coast to ~45 km due to 10-15 km of underplating as a consequence of magma upwelling.

Plain language summary

The Deccan Traps, in western India, is a continental flood basalt province. The volcanism occurred around 65 million years (Ma) ago when India was in the southern latitude. While moving northward, India interacted with the Reunion hotspot, leading to increased mantle temperature and consequent melting. Due to buoyancy, the magma moved upward and ponded towards the crust-mantle boundary. When the magma in these lower crustal or Moho-depth chambers is buoyant and overpressures are high enough to cause the overlying crust to fail, it will ascend via dikes and assimilate into a shallow crust. The process is expected to produce significant crustal modification due to increased heat transfer from the mantle to the surface and chemical transformation. Existing geophysical knowledge of the Deccan traps does not provide evidence for such crustal transformations. Using data from a high-density seismic experiment to construct a detailed model of the crust, we discovered magma ponding at the crust-mantle boundary beneath the coastal basin, an extensive low-velocity layer in the upper/mid crust possibly representing the horizontally elongated frozen magma reservoir, and a densified high-velocity layer in the shallow crust (at a depth of 4-8 km) representing basaltic mafic intrusions.

1.0 Introduction

Understanding the location and form of magma storage in the crust is important to model fundamental Earth processes such as crustal growth, ore deposit formation, and predicting geohazards related to volcanism (Hill et al., 1991; Richards et al., 1989; Self et al.,

2008). The generation of magma requires two operations: the partial melting of rocks, either by supplying heat or by reducing the pressure and consequently changing the solidus temperature; and the melt separation from the residual solid matrix through relative motion between the matrix and the melt (McKenzie, 1984). The conceptual model for continental flood basalt, first proposed by Cox (1980), includes magma's origin in the mantle, most likely due to the interaction of mantle plumes at the base of the lithosphere, followed by the melt rising towards the base of the crust, where rheological and density contrasts may cause the melt to pond and form large primitive magma chambers (Ridley & Richards, 2010). When the magma in these chambers at lower crust or Moho depth is buoyant and overpressures are high enough to cause the failure of the overlying crust, it will ascend via dikes and assimilate at a shallow crustal depth (e.g., Bachmann & Huber, 2016; Black et al., 2021; Sparks et al., 1984).

Geophysical techniques have been successfully used in investigating the structure of the magma plumbing in active volcanic systems (e.g., Chrapkiewicz et al., 2022; Jaxybulatov et al., 2014; Lees, 2007; Paulatto et al., 2022; Peng & Humphreys, 1998; Ward et al., 2014). This knowledge helps in providing critical insights into magma emplacement, mush evolution, and modelling the quantum of CO_2 outflux (e.g., Cartwright & Hansen, 2006; Kasbohm, 2022; Muirhead et al., 2014; Tian & Buck, 2022). Geophysical imaging of old volcanic systems like the Deccan, Columbia, and Siberia is, however, more difficult and debated due to weak geophysical signatures as a consequence of magma solidification because of heat loss.

The Deccan Volcanic Province (DVP) is a Large Igneous Province (LIP) encompassing an area of about a half-million km^2 in west-central India (Figure 1a), with a possible extension of an additional one million km^2 beneath the Arabian Sea to the west (Colleps et al., 2021; Jay & Widdowson, 2008; Sen, 2001). The volcanism in DVP was the consequence of the interaction of the fast-moving Indian plate with the Reunion mantle plume in the southern latitude at around 65 Ma (Mahoney, 1988; Morgan, 1972). The basalt attains a maximum thickness of 1.5-2 km along the Western Ghat escarpment (Holmes, 1965) and thins eastward. To the west of the escarpment is the narrow, flat coastal plain that is divided by an N-S extensional fault referred to as the Panvel Flexure (Figure 1b). The nature and genesis of the Panvel Flexure are debated (Dessai & Bertrand, 1995). The DVP is one of the most interesting subjects of research for three principal reasons: its enormous size, a

typical area to understand the process of magmatism in the planetary system, and a unique case for solid earth-climate interaction leading to major mass extinction and rapid climate change. A series of recent papers (e.g., Krishnamurthy et al., 2000; Mittal et al., 2021; Nava et al., 2021; Self et al., 2022) provide a detailed review of the subject.

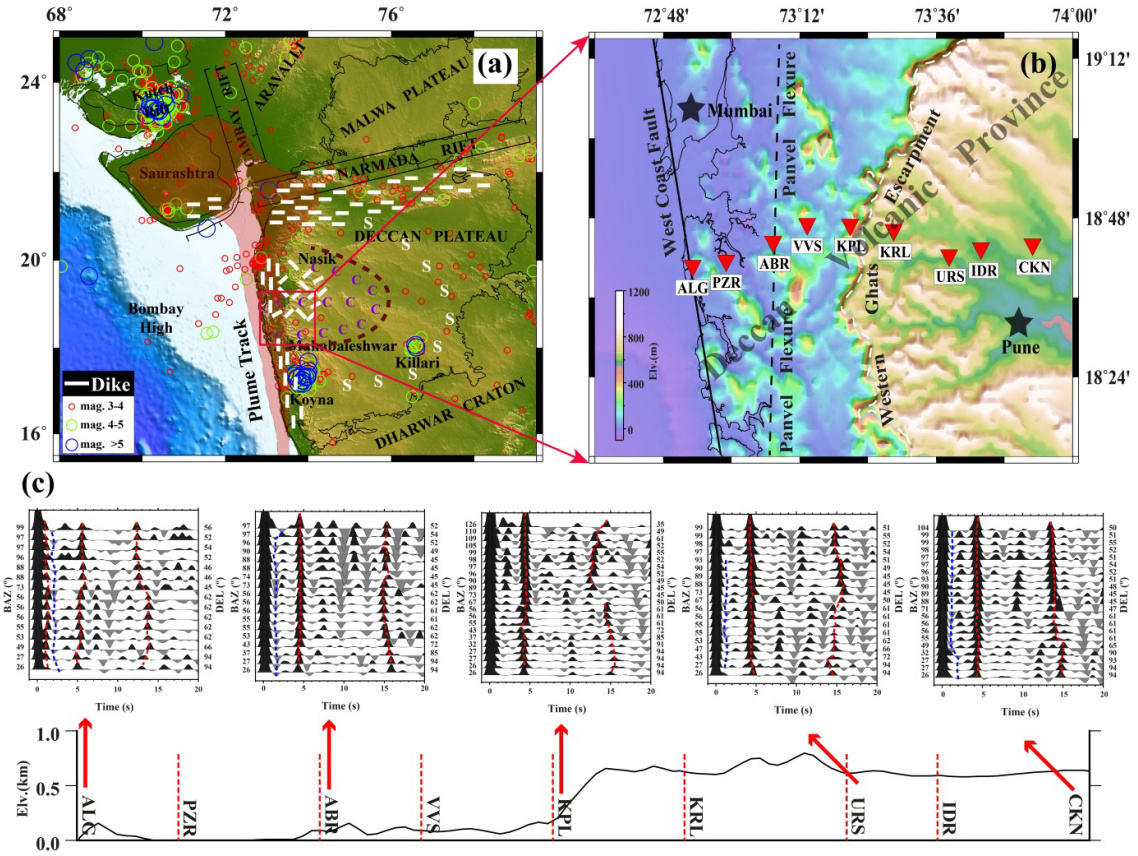

Figure 1. Map of the study area and the data set used. (a) A topographic map of the DVP and surrounding area. Local seismicity is shown in circles. The pink shade along the west coast represents the mantle plume track. White dashed lines indicate dikes. The area marked as "C" indicates compound magma flow, and that marked as "S" indicates simple flow (Sen, 2001; Sen & Chandrasekharam, 2011). (b) Location of broadband seismological stations operated during 2020-21, along with important tectonic features. (c) A plot of selected RFs with varying earthquake distance and back azimuth for selected stations.

Numerous geophysical experiments have been performed over the DVP to investigate its crustal structure. None of them, however, show evidence of an upper-crustal magma chamber beneath it (e.g., Bhattacharji et al., 2004; Chopra et al., 2014; Kaila et al., 1981;

Krishna et al., 1991; Mohan & Kumar, 2004; Patro & Sarma, 2016; Patro et al., 2018; Prasad et al., 2018; Tiwari et al., 2001). Some of these studies do indicate the presence of magma underplating, albeit with poorly quantified thickness, location, velocity, and density. We present here the first evidence and location of the possible magma ponding in the lower crust, and the shallow magma chamber through seismic imaging of the crust beneath the western segment of the DVP adjoining the west coast of India using broadband seismic waveform data (Figure 1b). Our inference is based on the joint inversion of receiver function and surface wave dispersion data (Julia et al., 2000), supported by the modelling of ambient noise data (e.g., Shapiro et al., 2005).

2.0 Data and preliminary analysis

We deployed 9 broadband seismographs (Figure 1b) aligned W-E from the west coast of India, between January 2020 and September 2021, with an inter-station spacing of 10-15 km. The experiment was executed in the region of the final Deccan eruption, where the magma chamber is hypothesized based on the analysis of megacrysts in the Giant Plagioclase Basalts (Higgins & Chandrasekharam, 2007). The region has a large number of dikes and compound magma flows (Figure 1a). The P receiver functions (RFs) were computed for selected earthquakes of magnitudes above 5.5 and epicenter distances between 30° and 95° (Figure S1 a, b) using a time domain iterative deconvolution approach (Ligorría & Ammon, 1999). A low-pass Gaussian filter was applied with a parameter of 2.5, which means the corresponding cut-off frequency is ∼1.2 Hz and the pulse width of ∼1.0 s. These RFs were used to compute the structural model using Common Conversion Point (CCP) migration (Dueker & Sheehan, 1997) and perform inversion jointly with Rayleigh wave group velocity dispersion (e.g., Julia et al., 2000).

A sample of RFs at a few locations is presented in Figure 1c. Important features of the RFs are a positive conversion at about ~0.5 s, a negative one at ~1.5 s, and a Moho converted phase at 4.5-5.5 s. To analyse the shallow depth conversions in detail, we computed RF at a location for varying Gaussian widths from 2.5 to 15, corresponding to a maximum frequency content of 1.2 Hz to 6 Hz (Figure S1c). Here, the P phase arrival (L1) is delayed by 0.1 s which suggests the presence of a thin low-velocity layer possibly due to the Deccan basalt with Vs of 1.8-2.4 km/s and a thickness of about 1 km (Ray et al., 2021). A positive P-S conversion at 0.6 s (L2) represents a 4-5 km thick high-velocity layer. Further, a low-velocity layer (LVL) in the upper crust is identified by two P-to-S converted phases at 1.4 s and 1.7 s (L3 & L4) due to the conversion from the top and bottom of the LVL. The approximate

location of the LVL is between 10 and 16 km. The Moho converted phase is identified at about 4.5 s (marked as M), corresponding to a depth of about 36 km. A plot of the RFs time series along the profile for an earthquake (Figure S1d) shows the presence of these features, albeit with local variations in layer depth and velocity contrast. The RFs along the profile show the delayed arrival time of the Moho conversion with a reduced amplitude below the coastal stations, particularly the two westernmost stations. To quantify these parameters, we modelled receiver function data, as discussed in subsequent sections.

3.0 Methodology and result

3.1 Joint inversion of receiver function and surface wave data

To map the interface depth and provide a reliable velocity image, we perform an inversion of the RF time series with the surface wave dispersion data (e.g., Julia et al., 2000) using an iterative sequence of linearized least squares inversions (Herrmann & Ammon, 2002). Details of the methodology are provided in Supplementary Text S1. The velocity model at individual stations presented in Figures S2 and S3 is interpolated to generate a W-E velocity profile to a depth of 60 km (Figure 2a). The Moho is identified by depth to maximum velocity gradients beyond the depth of 30 km and velocity beyond Vs of 4.3 km/s, corresponding to a typical peridotite P-velocity of >7.6 km/s. The Moho depth varies from 37 to 40 km, except in the coastal region, where it increases to about 45 km. Similar Moho depths are obtained using H-K stacking as well (Figure S4). A thick (10-15 km) underplated layer (UL) with Vs >4.0 km/s above the deeper part of Moho is mapped beneath the west coast, compared with 3-5 km thickness elsewhere. A high-velocity layer (HVL) of Vs 3.7-3.9 km/s is identified in the shallower part (4-8 km) lying over the prominent low-velocity layer (LVL) in the depth range of 8 to 17 km with Vs of 3.3-3.5 km/s.

We performed a number of forward models to ascertain the robustness of the Moho depth, the high-velocity underplating layer, and low and high velocities in the shallower crust (Figure S5 a-d). To examine the continuity of the LVL in other parts of the DVP, we modelled data from regionally distributed stations (Figure S6). The result shows no evidence for such an LVL away from the study region. In the absence of a well-distributed network, we are unable to delineate the zone with the LVL in the shallow crust.

3.2 Receiver function imaging

We create a depth image of impedance contrast below the profile using the Common Conversion Point (CCP) stacking method (Dueker & Sheehan, 1997). The CCP stacks are constructed by back-projecting each RF time series to its appropriate spatial location in depth using ray theory and a shear wave velocity model (and a Vp/Vs of 1.74) derived from a joint inversion for the easternmost station, CKN (Figure 1b). The spatial location of the converted phase at depths of 10, 30, and 50 km is presented in Figure S7. To successfully image structure that varies along the section, the Fresnel zones must overlap by ~50% or more at the depth of interest (Zhai & Levander, 2011). The Fresnel zone width for Ps at 10, 30, and 50 km depth is ~4, 6, and 12 km. The RF stack is computed in a bin of 5 km width and every 1 km depth and further smoothened over 10 km horizontal window. The CCP image coherently stacks RF phase conversions and also partially cancels random noise. The CCP image (Figure 2b) reveals three characteristic features: a positive conversion (HVL) at about 5 km, underlain by a negative conversion (LVL) at ~10 km, and the Moho depth of 35-40 km that increases to ~45 km below the coastal plain. The Moho depth, determined using H-K stacking (Figure S4), is superimposed on the CCP image (Figure 2b). Three different approaches: joint inversion of RF and surface waves, CCP migration, and H-K stacking show very similar and consistent features.

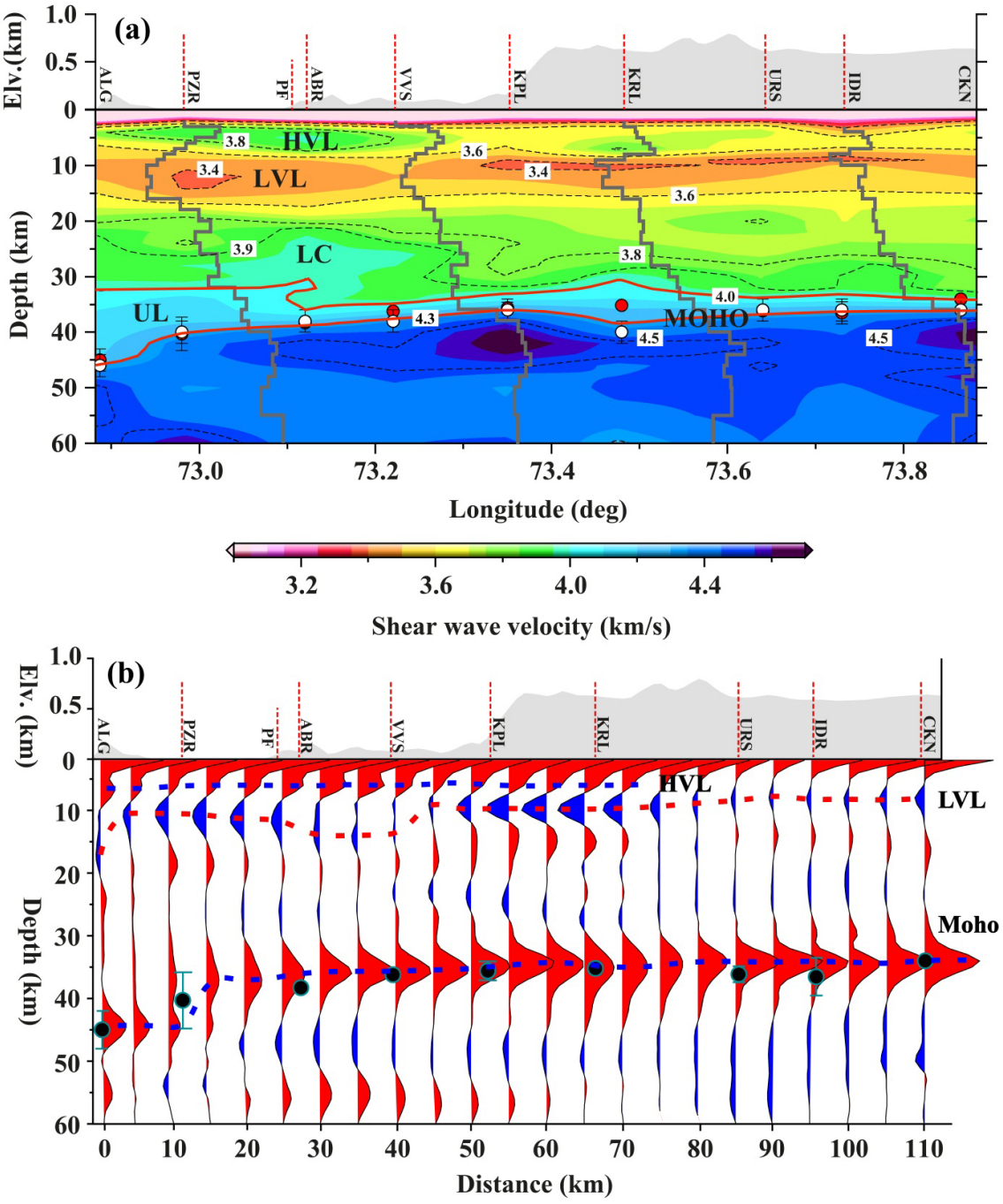

Figure 2. (a) Shear wave velocity profile created through the joint inversion of RF and surface wave dispersion data. Grey lines are 1D velocity models at selected stations. Red circles indicate the Moho from H-K stacking method (Figure S4) and the white circles are the Moho from joint inversion (Figure S3). HVL-High velocity layer, LVL-Low velocity layer, LC-Lower crust (Vs >3.8-4.0 km/s), UL-Underplated layer (Vs>4.0 km/s), PF-Panvel

Flexure. (b) CCP image along the seismic profile. Black circles are the Moho estimates from H-K stacking (Figure S4).

4.0 Discussion

A velocity-depth section of the crust along a ~106 km long profile from the west coast of the DVP in west-central India is presented in Figure 2a. We examine the possible alteration in Pre-Deccan crust in Figure 3a due to the volcanism. Deep drill hole samples from the Koyna region, about 100 km south of this profile, show that the basement of the DVP closely resembles the Dharwar craton (Ray et al, 2021; Shukla et al., 2022). An ensemble of velocity models (Figure 3a) of the DVP along the profile, compared with the Dharwar craton (Borah et al., 2014; Chaubey et al., 2022), suggests significant differences between the crustal properties: a lower velocity at a depth of 8-17 km and a higher velocity at 4-8 km below the seismic profile in the DVP. We observe a laterally variable underplated basal layer (Vs >4.0 km/s) in the lower crust. The Moho depth is mapped at ~35 km along the profile, except beneath the west coast over a distance of 40 km, where it deepens to ~45 km. The deep Moho zone beneath the coastal plain coincides with significant magma underplating of ~10-15 km and terminates in the east below the Panvel Flexure. We discuss the significance of these features below.

4.1 The lower crust and uppermost mantle

The Deccan magmas were produced by high-temperature melting at a depth of 60-100 km (Sen, 2001), located beneath the west coast of India and underlying regions of uplift in dynamic topography (Glišović & Forte, 2017). Existing seismological observations are inadequate to define the spatial extent of high mantle temperatures. Iyer et al. (1989), based on travel-time modelling of teleseismic rays, proposed that most of the DVP is underlain by a thick continental root, except for the westernmost part adjoining the west coast. Being at the edge of the craton, this segment of the DVP has thin lithosphere and was most influenced by the Réunion hot spots (Sharma et al., 2018). The mantle melting led to magma ponding at the base of the crust, which eventually resulted in high-velocity underplating and crustal thickening as observed in the coastal plain. The Moho is about 10-15 km thicker beneath the west coast due to the presence of an underplated layer with Vs > 4.0 km/s (Figure 2a), as expected from the presence of solidified olivine and clinopyroxene rich cumulates in deep magma reservoirs (Cox, 1993). Interestingly, we don’t observe magma underplating to the east of the western Ghat (about 60 km from the coast), which correlates well with

196 seismological evidence for undisturbed lithospheric mantle in the DVP to the east of the
197 western Ghat (Iyer et al., 1989; Kumar & Mohan, 2005).

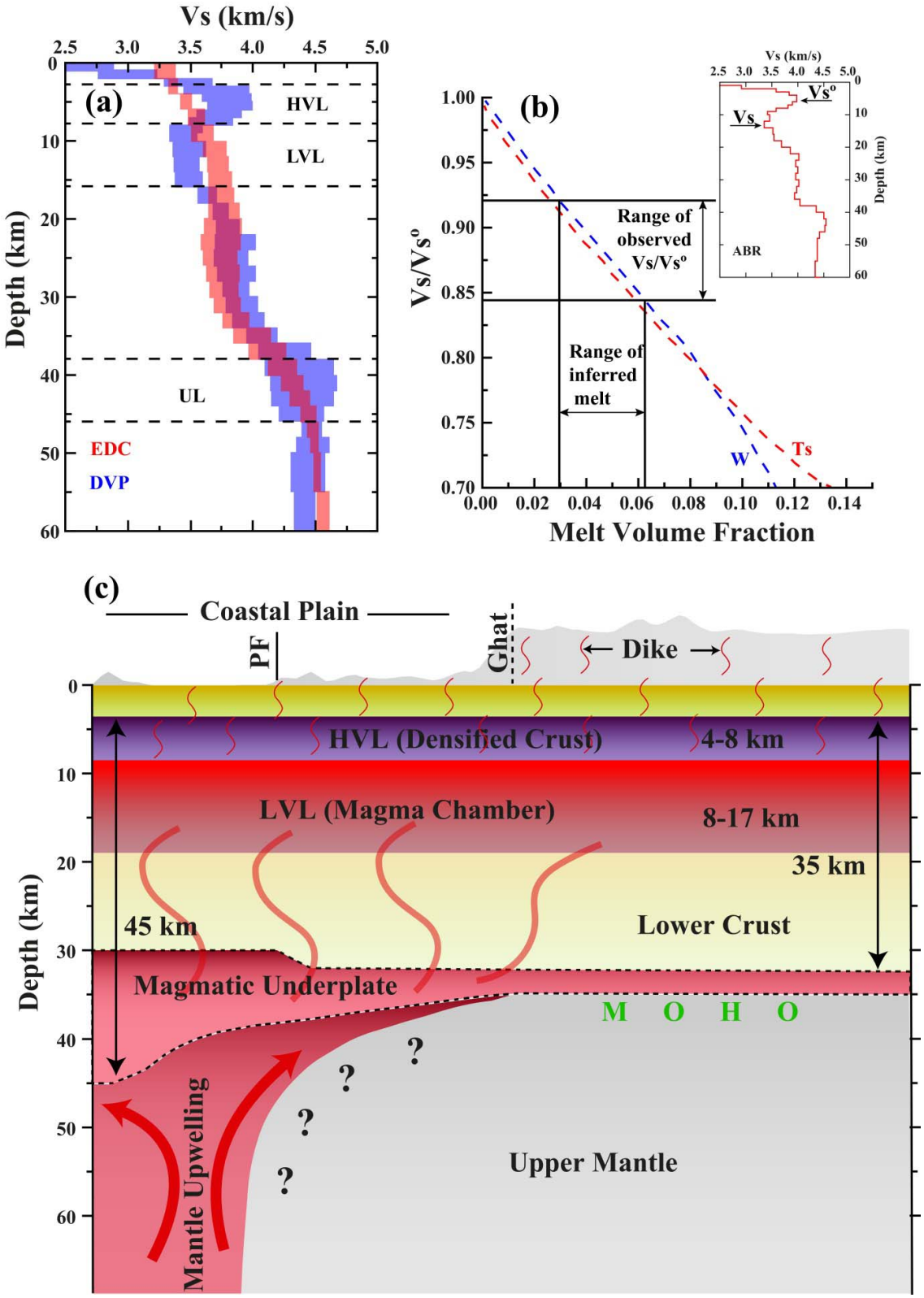

Figure 3. (a) Plot of an ensemble of velocity models for seismic stations located in the DVP and Dharwar craton. HVL-High velocity layer, LVL-Low velocity layer, UL-Underplated layer. (b) Proportional velocity reduction (Vs/Vs°) versus melt volume fraction. Horizontal lines indicate proportional velocity reductions in the low-velocity layer (LVL) for the regions. W: blue line is an analytical relationship of Watanabe (1993) for randomly oriented triangular melt tubes. Ts: Red dashed line is an analytical relationship of Taylor and Singh (2002) for the slow propagation direction in a medium containing perfectly aligned oblate spheroids of aspect ratio 10. (c) Schematic view of the magmatic system beneath the DVP coinciding with seismic profile in Figure 1b. The thick red arrow indicates the ascending direction of the melts from the upper mantle to the crust-mantle boundary. PF is Panvel Flexure.

198 4.2 Low velocity in upper crust

199 At a depth of 8 to 17 km, we observe an approximately 0.1-0.4 km/s (or 3-12%)
200 velocity reduction (Vs ~3.3-3.5 km/s) relative to the Dharwar Craton (Vs ~3.7 km/s). Such
201 low velocity in the shallow crust has been reported in various geological settings as a
202 consequence of crustal rejuvenation in cratonic regions, partial melting, felsic composition,
203 or strong radial anisotropy (Beck & Zandt, 2002; Diaferia & Cammarano, 2017; Gao et al.,
204 2020; Kind et al., 1996; Li et al., 2003; Ward et al., 2014; Zheng et al., 2015; Zorin et al.,
205 2003).

206 A global compilation of experimentally measured shear wave velocities of dry rocks
207 (Christensen, 1996) at room temperature and lithostatic pressure of 400 MPa, corresponding
208 to a depth of about 12 km, suggests only a few rocks like Andesite (Vs~ 3.1 km/s); Basalt
209 (Vs~ 3.3 km/s); Slate (Vs~ 3.3 km/s); Phyllite (Vs~ 3.5 km/s); Granite Gneiss (Vs~ 3.6 km/s)
210 fall in the observed velocity range. To extrapolate these velocities to mid-crustal
211 temperatures, we used a Vs decrease of 0.2 m/s/°C, an average value determined from a range
212 of gneisses (Kern et al., 2001). Heat flow estimates in the neighbouring Koyna region (Figure
213 1a) from a 1,500 m deep borehole yielded an average value of 45 mW/m^2 (Ray et al., 2021).
214 Deep drilling confirms that the Deccan trap is underlain by granitoid rocks (TTG). Their 1-D
215 steady-state thermal modelling indicates temperatures could vary from 165°C to 250°C at 10
216 km depth, much higher than previously reported. These results depend on the assumed
217 thermal conductivity of the underlying rock and should be used cautiously. Therefore,
218 although higher temperature is possibly a contributing factor, it may not be the only cause of
219 the observed low upper-crustal velocity.

The LVL could also be due to the presence of partial melts, aqueous fluids, or both since these are easily capable of a velocity decrease of 7–17% (Takei, 2000; Watanabe, 1993). To constrain the percentage of melt present in the DVP, we compared our shear-wave velocities with theoretical and experimentally-derived relationships between Vs and melt percentage (Figure 3b). We used the ratio of Vs to Vs°, which represents the minimum of the LVL and the upper-crustal peak velocity, respectively, for the velocity profile at each station (Figure 2a). Using Figure 3b, we obtain the presence of a moderate to low melt percentage (3-6%) corresponding to the LVL. In a detailed thermodynamic model considering anhydrous and two wet components, Diaferia and Cammarano (2017) inferred that the Vs at 400 MPa is influenced more by the presence of melt compared to water. They concluded that Vs <3.6 km/s in the crystalline crust would imply a strong contribution of sediment and/or melt. Additionally, deep magmas were transported upward through the crust via the development and propagation of faults (Downs et al., 2018), and some liquid and/or gas could have migrated into these faults, changing the physical properties of the nearby rocks. Thus, partial melt and fluid-filled faults are significant causes for producing the crustal low-velocity zone below magmatic provinces.

The other factor influencing shear wave velocity is the seismic anisotropy in the Earth's crust, observed in almost all geological and tectonic settings (e.g., Illsley-Kemp et al., 2021; Johnson et al., 2011; Li & Peng, 2017; Savage et al., 2017). It is caused by structural features such as faults (Zinke & Zoback, 2000), and aligned melt pockets (e.g., Bastow et al., 2010; Dunn et al., 2005; Keir et al., 2005, 2011), where the polarization direction is parallel to the trend of structural features. In the upper crystalline crust, where anisotropy is generally weak, it is explained by micro-cracking often related to present day stress and also mineral fabric. In the middle and lower crust, it is generally attributed to rock texture, like mineral alignment from sheared and metamorphosed rock. Mahan (2006) argued that deformed granitic rocks may also have a significant increase in mica content due to the breakdown of feldspar or fluid related mass transfer and can have significant anisotropy. Seismic anisotropy has been inferred in dikes or sill complexes where fine-scale layering affects the macro-mechanical properties of the crustal material. Tectonically active regions (Shapiro et al., 2004; Moschetti et al., 2010), and volcanic regions (Jaxybulatov et al., 2014) show well defined anisotropy related to the horizontal layering associated with mineralogical preferential orientation. We present here the first report of crustal anisotropy using limited data.

Simultaneous inversion of the dispersion curves of Rayleigh and Love surface waves has been widely used to estimate radial anisotropy in the crust using dispersion measurements at periods <20 s, which is possible with the correlation of the ambient seismic noise field (Shapiro et al., 2005). Following this approach, Das and Rai (2017) inferred 3% anisotropy in the upper and middle crust of the Dharwar craton. Due to the short length of the present profile, we could only retrieve Rayleigh and Love wave phase velocity dispersion data up to 20 s through cross-correlation of the ambient noise field only for two inter-station pairs (Figure S8a). An inversion of dispersion data for these two pairs (Figures S8 b, c) shows the presence of positive radial anisotropy (Vsh>Vsv) in the depth of 8-17 km, where the low velocity is inferred. The magnitude of the anisotropy ranges from 5-15%, indicating the possible contribution of mineral alignment in the horizontal directions during the magma flow, leading to Vs reductions in the LVL layer as discussed earlier.

4.3 High velocity in the shallow crust

Our velocity model shows the presence of shear velocities of 3.7-3.9 km/s in the depth range of 4-8 km, in contrast with the 3.5 km/s observed over the Dharwar craton, which is higher by 0.2-0.4 km/s (5-10%). The first observation of such a high velocity upper crust in DVP was made by Rai et al. (1999) using local earthquake tomography in the neighbouring Koyna region. The high velocity at shallow depths is at odds with the general understanding of continental crust composition, where density generally increases with depth. Assuming a shear velocity-density relation (Brocher, 2005), we infer a high-density layer in the upper crust underlain by a low density one. The denser crust beneath the DVP section is probably due to basaltic crustal intrusions. Tian and Buck (2022) provide a detailed account and reference for extensive mafic intrusion beneath the Columbia River Basalt, Emeishan, Siberian, and Etendeka LIPs, based on geophysical data modelling. They suggest that crustal densification due to voluminous magma intrusion and solidification is necessary for the extrusion of continental flood basalts. Further, crystallization of such pre-eruption intrusions could release enough carbon dioxide to drive substantial global warming before the main phase of flood basalt volcanism. We speculate a similar scenario over the DVP, and the mapped HVL could have been the possible source region for large CO_2 releases.

Figure 3c provides a schematic view of the magma plumbing system beneath the DVP as a 2-D W-E oriented cross-section. The mafic magma originates from the upper mantle beneath the west coast and the adjoining sea, ascending in the lower crust to the upper-middle

crust. It is ponded at the crust-mantle boundary. A part of the magma intruded into the shallower crust, where it was densified and preserved as a high-velocity layer.

5 Conclusion

We constructed a high resolution crustal velocity model for the ~106 km length of the west-to-east transect, covering part of the Deccan traps from its west coast, using the seismological data at ~10-15 km intervals. We jointly inverted the P-receiver function with surface wave dispersion data. Also, we generated a 1-D velocity anisotropy model to a depth of 25 km from the analysis of two inter-station ambient noise paths. The velocity image provides evidence for a 10-15 km thick high-velocity layer (Vs>4.0 km/s) at the base of the crust, interpreted as a response of dense mafic underplating during magmatism at ~65 Ma and confined to a distance of 40 km only from the coast. In the shallower crust (8-17 km depth), a continuous low-velocity (Vsv of 3.3-3.5 km/s) and radially anisotropic (Vsh ~4 km/s) layer is mapped. This low velocity anisotropic layer possibly represents the horizontally elongated frozen magma reservoir, a source for the magma eruption. The low velocity layer underlies a densified high velocity isotropic layer with Vsv>3.8 km/s at a depth of 4-8 km, representing basaltic mafic intrusions responsible for the production of massive CO_2 degassing.

To improve the magma evolution process beneath the Deccan Volcanic Province, other physical properties of the crust, such as seismic anisotropy, attenuation, temperature, and the Vp/Vs ratio, are needed and are a subject to future investigations.

6 Acknowledgements

We gratefully appreciate the financial support from the Department of Atomic Energy, India in form of a Raja Ramanna Fellowship to SSR and Research Associateship to VK (research grant no. 1003/2021/RRF/R&DII). The field support from Vikrant Bartakke and Vibhas Shevde is greatly appreciated. The Department of Earth & Climate Science, IISER Pune provided generous support towards the field experiment. SSR thanks, Profs. Vinod Gaur, Kanchan Pande, Raymond Duraiswami, and Vivek Kale for many useful discussions on geological aspects of Deccan volcanism and magma plumbing.

7. Data availability statement

Receiver functions, surface wave dispersion, and velocity model at each station are provided as supplementary documents for a peer review process. After acceptance, these data will be made available on a public repository i.e., Zenodo.org.

8. References

Bachmann, O., & Huber, C. (2016). Silicic magma reservoirs in the Earth's crust. *American Mineralogist*, *101*(11), 2377-2404. https://doi.org/10.2138/am-2016-5675

Bastow, I. D., Pilidou, S., Kendall, J. M., & Stuart, G. W. (2010). Melt-induced seismic anisotropy and magma assisted rifting in Ethiopia: Evidence from surface waves. *Geochemistry, Geophysics, Geosystems*, *11*(6). https://doi.org/10.1029/2010GC003036

Beck, S. L., & Zandt, G. (2002). The nature of orogenic crust in the central Andes. *Journal of Geophysical Research: Solid Earth*, *107*(B10), ESE-7. https://doi.org/10.1029/2000JB000124

Bhattacharji, S., Sharma, R., & Chatterjee, N. (2004). Two-and three-dimensional gravity modeling along western continental margin and intraplate Narmada-Tapti rifts: Its relevance to Deccan flood basalt volcanism. *Journal of Earth System Science*, *113*(4), 771-784. https://doi.org/10.1007/BF02704036

Black, B. A., Karlstrom, L., & Mather, T. A. (2021). The life cycle of large igneous provinces. *Nature Reviews Earth & Environment*, *2*(12), 840-857. https://doi.org/10.1038/s43017-021-00221-4

Borah, K., Rai, S. S., Prakasam, K. S., Gupta, S., Priestley, K., & Gaur, V. K. (2014). Seismic imaging of crust beneath the Dharwar Craton, India, from ambient noise and teleseismic receiver function modelling. *Geophysical Journal International*, *197*(2), 748-767. https://doi.org/10.1093/gji/ggu075

Brocher, T. M. (2005). Empirical relations between elastic wavespeeds and density in the Earth's crust. *Bulletin of the seismological Society of America*, *95*(6), 2081-2092. https://doi.org/10.1785/0120050077

Cartwright, J., & Hansen, D. M. (2006). Magma transport through the crust via interconnected sill complexes. *Geology*, *34*(11), 929-932. https://doi.org/10.1130/G22758A.1

Chaubey, D. K., Rai, S. S., Mullick, N., & Das, R. (2022). Unperturbed Archean lithosphere beneath the Eastern Dharwar Craton Kimberlite Field, India: inferred from joint inversion of surface wave dispersion and receiver function data. *Precambrian Research (in review)*. https://doi.org/10.1002/essoar.10512636.1

Chopra, S., Chang, T. M., Saikia, S., Yadav, R. B. S., Choudhury, P., & Roy, K. S. (2014). Crustal structure of the Gujarat region, India: New constraints from the analysis of teleseismic receiver functions. *Journal of Asian Earth Sciences*, *96*, 237-254. https://doi.org/10.1016/j.jseaes.2014.09.023

Chrapkiewicz, K., Paulatto, M., Heath, B., Hooft, E., Nomikou, P., Papazachos, C., & Morgan, J. (2022). Magma chamber detected beneath an arc volcano with high-resolution velocity images. *submitted to EarthArXiv*. https://doi.org/10.31223/X5934R

Christensen, N. I. (1996). Poisson's ratio and crustal seismology. *Journal of Geophysical Research: Solid Earth*, *101*(B2), 3139-3156. https://doi.org/10.1029/95JB03446

Colleps, C. L., McKenzie, N. R., Guenthner, W. R., Sharma, M., Gibson, T. M., & Stockli, D. F. (2021). Apatite (U-Th)/He thermochronometric constraints on the northern extent of the Deccan large igneous province. *Earth and Planetary Science Letters*, *571*, 117087. https://doi.org/10.1016/j.epsl.2021.117087

Cox, K. G. (1980). A model for flood basalt volcanism. *Journal of Petrology*, *21*(4), 629-650. https://doi.org/10.1093/petrology/21.4.629

Cox, S. (1993). Inter-related plutonism and deformation in South Victoria Land, Antarctica. *Geological Magazine, 130*(1), 1-14. https://doi.org/10.1017/S0016756800023682

Das, R., & Rai, S. S. (2017). Extensive seismic anisotropy in the lower crust of Archean metamorphic terrain, South India, inferred from ambient noise tomography. *Tectonophysics*, *694*, 164-180. https://doi.org/10.1016/j.tecto.2016.12.002

Dessai, A. G., & Bertrand, H. (1995). The “Panvel Flexure” along the Western Indian continental margin: an extensional fault structure related to Deccan magmatism. *Tectonophysics*, *241*(1-2), 165-178. https://doi.org/10.1016/0040-1951(94)00077-M

Diaferia, G., & Cammarano, F. (2017). Seismic signature of the continental crust: what thermodynamics says? An example from the Italian Peninsula. *Tectonics*, *36*(12), 3192-3208. https://doi.org/10.1002/2016TC004405

Downs, D. T., Stelten, M. E., Champion, D. E., Dietterich, H. R., Nawab, Z., Zahran, H., & Shawali, J. (2018). Volcanic history of the northernmost part of the Harrat Rahat volcanic field, Saudi Arabia. *Geosphere*, *14*(3), 1253-1282. https://doi.org/10.1130/GES01625.1

Dueker, K. G., & Sheehan, A. F. (1997). Mantle discontinuity structure from midpoint stacks of converted P to S waves across the Yellowstone hotspot track. *Journal of Geophysical Research: Solid Earth*, *102*(B4), 8313-8327. https://doi.org/10.1029/96JB03857

Dunn, R. A., Lekić, V., Detrick, R. S., & Toomey, D. R. (2005). Three-dimensional seismic structure of the Mid-Atlantic Ridge (35 N): Evidence for focused melt supply and lower crustal dike injection. *Journal of Geophysical Research: Solid Earth*, *110*(B9). https://doi.org/10.1029/2004JB003473

Gao, H., Yang, X., Long, M. D., & Aragon, J. C. (2020). Seismic evidence for crustal modification beneath the Hartford rift basin in the northeastern United States. *Geophysical Research Letters*, *47*(17), e2020GL089316. https://doi.org/10.1029/2020GL089316

Glišović, P., & Forte, A. M. (2017). On the deep-mantle origin of the Deccan Traps. *Science*, *355*(6325), 613-616. https://doi.org/10.1126/science.aah4390

Herrmann, R. B., & Ammon, C. J. (2002). Computer programs in seismology: Surface waves, receiver functions and crustal structure. *St. Louis University, St. Louis, MO*, *25*, 46. http://www.eas.slu.edu/People/RBHerrmann/CPS330.html

Higgins, M. D., & Chandrasekharam, D. (2007). Nature of sub-volcanic magma chambers, Deccan Province, India: evidence from quantitative textural analysis of plagioclase

megacrysts in the Giant Plagioclase Basalts. *Journal of Petrology*, *48*(5), 885-900. https://doi.org/10.1093/petrology/egm005

Hill, R. I., Campbell, I. H., & Griffiths, R. W. (1991). Plume tectonics and the development of stable continental crust. *Exploration Geophysics*, *22*(1), 185-188. https://doi.org/10.1071/EG991185

Holmes, A., 1965, Principles of Physical Geology, Thomas Nelson & Sons, London, 1288 p.

Illsley-Kemp, F., Barker, S. J., Wilson, C. J., Chamberlain, C. J., Hreinsdóttir, S., Ellis, S., & Wadsworth, F. B. (2021). Volcanic unrest at Taupō volcano in 2019: Causes, mechanisms and implications. *Geochemistry, Geophysics, Geosystems*, *22*(6), e2021GC009803. https://doi.org/10.1029/2021GC009803

Iyer, H. M., Gaur, V. K., Rai, S. S., Ramesh, D. S., Rao, C. V. R., Srinagesh, D., & Suryaprakasam, K. (1989). High velocity anomaly beneath the Deccan volcanic province: Evidence from seismic tomography. *Proceedings of the Indian Academy of Sciences-Earth and Planetary Sciences*, *98*(1), 31-60. https://doi.org/10.1007/BF02880375

Jaxybulatov, K., Shapiro, N. M., Koulakov, I., Mordret, A., Landès, M., & Sens-Schönfelder, C. (2014). A large magmatic sill complex beneath the Toba caldera. S*cience*, *346*(6209), 617-619. https://doi.org/10.1126/science.1258582

Jay, A. E., & Widdowson, M. (2008). Stratigraphy, structure and volcanology of the SE Deccan continental flood basalt province: implications for eruptive extent and volumes. *Journal of the Geological Society*, *165*, 177-188. https://doi.org/10.1144/0016-76492006-062

Johnson, J. H., Savage, M. K., & Townend, J. (2011). Distinguishing between stress-induced and structural anisotropy at Mount Ruapehu Volcano, New Zealand. *Journal of Geophysical Research: Solid Earth*, *116*(B12). https://doi.org/10.1029/2011JB008308

Julia, J., Ammon, C. J., Herrmann, R. B., & Correig, A. M. (2000). Joint inversion of receiver function and surface wave dispersion observations. *Geophysical Journal International*, *143*(1), 99-112. https://doi.org/10.1046/j.1365-246x.2000.00217.x

425 Kaila, K. L., Reddy, P. R. Dixit, M. M, & Lazarenko, M. A. (1981). Deep crustal structure at
426 Koyna, Maharashtra, indicated by deep seismic soundings. *Journal of the*
427 *Geologicical Society of India, 22* (1) 1-16.

428 Kasbohm, J. (2022). Flood basalt buildup warms climate. *Nature Geoscience*, *15*(5), 342-
429 343. https://doi.org/10.1038/s41561-022-00944-z

430 Keir, D., Kendall, J. M., Ebinger, C. J., & Stuart, G. W. (2005). Variations in late syn-rift
431 melt alignment inferred from shear-wave splitting in crustal earthquakes beneath the
432 Ethiopian rift. *Geophysical Research Letters*, *32*(23).
433 https://doi.org/10.1029/2005GL024150

434 Keir, D., Belachew, M., Ebinger, C. J., Kendall, J. M., Hammond, J. O., Stuart, G. W., &
435 Rowland, J. V. (2011). Mapping the evolving strain field during continental breakup
436 from crustal anisotropy in the Afar Depression. *Nature Communications*, *2*(1), 1-7.
437 https://doi.org/10.1038/ncomms1287

438 Kern, H., Popp, T., Gorbatsevich, F., Zharikov, A., Lobanov, K. V., & Smirnov, Y. P. (2001).
439 Pressure and temperature dependence of Vp and Vs in rocks from the superdeep well
440 and from surface analogues at Kola and the nature of velocity anisotropy.
441 *Tectonophysics*, *338*(2), 113-134. https://doi.org/10.1016/S0040-1951(01)00128-7

442 Kind, R., Ni, J., Zhao, W., Wu, J., Yuan, X., Zhao, L., & Hearn, T. (1996). Evidence from
443 earthquake data for a partially molten crustal layer in southern Tibet. *Science*,
444 *274*(5293), 1692-1694. https://doi.org/10.1126/science.274.5293.1692

445 Krishna, V. G., Kaila, K. L., & Reddy, P. R. (1991). Low velocity layers in the subcrustal
446 lithosphere beneath the Deccan Traps region of western India. *Physics of the Earth*
447 *and Planetary Interiors*, *67*(3-4), 288-302. https://doi.org/10.1016/0031-
448 9201(91)90025-D

449 Krishnamurthy, P., Gopalan, K., & Macdougall, J. D. (2000). Olivine compositions in picrite
450 basalts and the Deccan volcanic cycle. *Journal of Petrology*, *41*(7), 1057-1069.
451 https://doi.org/10.1093/petrology/41.7.1057

Kumar, M. R., & Mohan, G. (2005). Mantle discontinuities beneath the Deccan volcanic province. *Earth and Planetary Science Letters*, *237*(1-2), 252-263. https://doi.org/10.1016/j.epsl.2005.06.034

Lees, J. M. (2007). Seismic tomography of magmatic systems. *Journal of Volcanology and Geothermal Research*, *167*(1-4), 37-56. https://doi.org/10.1016/j.jvolgeores.2007.06.008

Li, S., Unsworth, M. J., Booker, J. R., Wei, W., Tan, H., & Jones, A. G. (2003). Partial melt or aqueous fluid in the mid-crust of Southern Tibet? Constraints from INDEPTH magnetotelluric data. *Geophysical Journal International*, *153*(2), 289-304. https://doi.org/10.1046/j.1365-246X.2003.01850.x

Li, Z., & Peng, Z. (2017). Stress-and structure-induced anisotropy in southern California from two decades of shear wave splitting measurements. *Geophysical Research Letters*, *44*(19), 9607-9614. https://doi.org/10.1002/2017GL075163

Ligorría, J. P., & Ammon, C. J. (1999). Iterative deconvolution and receiver-function estimation. *Bulletin of the seismological Society of America*, *89*(5), 1395-1400. https://doi.org/10.1785/BSSA0890051395

Mahan, K. (2006). Retrograde mica in deep crustal granulites: Implications for crustal seismic anisotropy. *Geophysical Research Letters*, *33*(24). https://doi.org/10.1029/2006GL028130

Mahoney, J. J. (1988). Deccan traps. In *Continental flood basalts* (pp. 151-194). Springer, Dordrecht. https://doi.org/10.1007/978-94-015-7805-9_5

McKenzie, D. P. (1984). The generation and compaction of partially molten rock. *Journal of Petrology*, *25*(3), 713-765. https://doi.org/10.1093/petrology/25.3.713

Mittal, T., Richards, M. A., & Fendley, I. M. (2021). The magmatic architecture of continental flood basalts I: Observations from the Deccan Traps. *Journal of Geophysical Research: Solid Earth*, *126*(12), e2021JB021808. https://doi.org/10.1029/2021JB021807

Mohan, G., & Kumar, M. R. (2004). Seismological constraints on the structure and composition of western Deccan volcanic province from converted phases. *Geophysical research letters*, *31*(2). https://doi.org/10.1029/2003GL018920

Morgan, W. J. (1972). Deep mantle convection plumes and plate motions. *AAPG bulletin*, *56*(2), 203-213. https://doi.org/10.1306/819A3E50-16C5-11D7-8645000102C1865D

Moschetti, M. P., Ritzwoller, M. H., Lin, F., & Yang, Y. (2010). Seismic evidence for widespread western-US deep-crustal deformation caused by extension. *Nature*, *464*(7290), 885-889. https://doi.org/10.1038/nature08951

Muirhead, J. D., Airoldi, G., White, J. D., & Rowland, J. V. (2014). Cracking the lid: Sill-fed dikes are the likely feeders of flood basalt eruptions. *Earth and Planetary Science Letters*, *406*, 187-197. https://doi.org/10.1016/j.epsl.2014.08.036

Nava, H.A., Black, B. A., Gibson, S. A., Bodnar, R. J., Renne, P. R., & Vanderkluysen, L. (2021). Reconciling early Deccan Traps CO_2 outgassing and pre-KPB global climate. *Proceedings of the National Academy of Sciences*, *118*(14), e2007797118. https://doi.org/10.1073/pnas.2007797118

Patro, P. K., & Sarma, S. V. S. (2016). Evidence for an extensive intrusive component of the Deccan Large Igneous Province in the Narmada Son Lineament region, India from three dimensional magnetotelluric studies. *Earth and Planetary Science Letters*, *451*, 168-176. https://doi.org/10.1016/j.epsl.2016.07.005

Patro, P. K., Raju, K., & Sarma, S. V. S. (2018). Some Insights into the Lithospheric Electrical Structure in the Western Ghat Region from Magnetotelluric Studies. *Journal of the Geological Society of India, 92*(5), 529-532. https:// doi: 10.1007/s12594-018-1062-z

Paulatto, M., Hooft, E., Chrapkiewicz, K., Heath, B., Toomey, D., & Morgan, J. (2022). Advances in seismic imaging of magma and crystal mush. *Frontiers in Earth Science, 10:970131.* https://doi.org/10.3389/feart.2022.970131

Peng, X., & Humphreys, E. D. (1998). Crustal velocity structure across the eastern Snake River Plain and the Yellowstone swell. *Journal of Geophysical Research: Solid Earth*, *103*(B4), 7171-7186. https://doi.org/10.1029/97JB03615

508 Prasad, K. N. D., Singh, A. P., & Tiwari, V. M. (2018). 3D upper crustal density structure of
509 the Deccan Syneclise, Central India. *Geophysical Prospecting*, *66*(8), 1625-1640.
510 https://doi.org/10.1111/1365-2478.12675

511 Rai, S. S., Singh, S. K., Sarma, P. V. S. S., Srinagesh, D., Reddy, K. N. S., Prakasam, K. S.,
512 & Satyanarayana, Y. (1999). What triggers Koyna region earthquakes? Preliminary
513 results from seismic tomography digital array. *Proceedings of the Indian Academy of*
514 *Sciences-Earth and Planetary Sciences*, *108*(1), 1-14.
515 https://doi.org/10.1007/BF02840820

516 Ray, L., Gupta, R. K., Chopra, N., Gopinadh, D., & Dwivedi, S. K. (2021). Thermal and
517 physical properties of Deccan basalt and Neoarchean basement cores from a deep
518 scientific borehole in the Koyna− Warna seismogenic region, Deccan Volcanic
519 Province, western India: Implications on thermal modeling and seismogenesis. *Earth*
520 *and Space Science*, *8*(10), e2021EA001645. https://doi.org/10.1029/2021EA001645

521 Richards, M. A., Duncan, R. A., & Courtillot, V. E. (1989). Flood basalts and hot-spot tracks:
522 plume heads and tails. *Science*, *246*(4926), 103-107.
523 https://doi.org/10.1126/science.246.4926.103

524 Ridley, V. A., & Richards, M. A. (2010). Deep crustal structure beneath large igneous
525 provinces and the petrologic evolution of flood basalts. *Geochemistry, Geophysics,*
526 *Geosystems*, *11*(9). https://doi.org/10.1029/2009GC002935

527 Saha, G., Rai, S. S., & Shalivahan. (2019). Occurrence of diamond in peninsular India and its
528 relationship with deep Earth seismic properties. *Journal of Earth System Science, 128*,
529 43. https://doi.org/10.1007/s12040-019-1088-7

530 Saha, G. K., Prakasam, K. S., & Rai, S. S. (2020). Diversity in the peninsular Indian
531 lithosphere revealed from ambient noise and earthquake tomography. *Physics of the*
532 *Earth and Planetary Interiors, 306*, 106523.
533 https://doi.org/10.1016/j.pepi.2020.106523

534 Savage, B., Covellone, B. M., & Shen, Y. (2017). Wave speed structure of the eastern North
535 American margin. *Earth and Planetary Science Letters*, *459*, 394-405.
536 https://doi.org/10.1016/j.epsl.2016.11.028

Self, S., Blake, S., Sharma, K., Widdowson, M., & Sephton, S. (2008). Sulfur and chlorine in Late Cretaceous Deccan magmas and eruptive gas release. *Science*, *319*(5870), 1654-1657. https://doi.org/10.1126/science.1152830

Self, S., Mittal, T., Dole, G., & Vanderkluysen, L. (2022). Toward Understanding Deccan Volcanism. *Annual Review of Earth and Planetary Sciences*, *50*, 477-506. https://doi.org/10.1146/annurev-earth-012721-051416

Sen, G. (2001). Generation of Deccan trap magmas. *Journal of Earth System Science*, *110*(4), 409-431. https://doi.org/10.1007/BF02702904

Sen, G., & Chandrasekharam, D. (2011). Deccan Traps Flood Basalt Province: An evaluation of the thermochemical plume model. In *Topics in igneous petrology* (pp. 29-53). Springer, Dordrecht. https://doi.org/10.1007/978-90-481-9600-5_2

Shapiro, N. M., Ritzwoller, M. H., Molnar, P., & Levin, V. (2004). Thinning and flow of Tibetan crust constrained by seismic anisotropy. *Science, 305*(5681), 233-236. https://doi.org/10.1126/science.1098276

Shapiro, N. M., Campillo, M., Stehly, L., & Ritzwoller, M. H. (2005). High-resolution surface-wave tomography from ambient seismic noise. *Science*, *307*(5715), 1615-1618. https://doi.org/10.1126/science.1108339

Sharma, J., Kumar, M. R., Roy, K. S., & Roy, P. N. S. (2018). Seismic imprints of plume-lithosphere interaction beneath the northwestern Deccan Volcanic Province. *Journal of Geophysical Research: Solid Earth*, *123*(12), 10-831. https://doi.org/10.1029/2018JB015947

Shukla, M. K., Vishnu, C. S., & Roy, S. (2022). Petrographic and geochemical characteristics of the granitic basement rocks below Deccan Traps obtained from scientific drilling to 3014 m depth in the Koyna region, western India. *Journal of Earth System Science*, *131*(2), 1-19. https://doi.org/10.1007/s12040-022-01888-z

Sparks, R. S. J., Huppert, H. E., & Turner, J. S. (1984). The fluid dynamics of evolving magma chambers. *Philosophical Transactions of the Royal Society of London. Series A, Mathematical and Physical Sciences*, *310*(1514), 511-534. https://doi.org/10.1098/rsta.1984.0006

566 Takei, Y. (2000). Acoustic properties of partially molten media studied on a simple binary
567 system with a controllable dihedral angle. *Journal of Geophysical Research: Solid*
568 *Earth*, *105*(B7), 16665-16682. https://doi.org/10.1029/2000JB900124

569 Taylor, M. A. J., & Singh, S. C. (2002). Composition and microstructure of magma bodies
570 from effective medium theory. *Geophysical Journal International*, *149*(1), 15-21.
571 https://doi.org/10.1046/j.1365-246X.2002.01577.x

572 Tian, X., & Buck, W. R. (2022). Intrusions induce global warming before continental flood
573 basalt volcanism. *Nature Geoscience*, *15*(5), 417-422. https://doi.org/10.1038/s41561-
574 022-00939-w

575 Tiwari V. M., Rao, M. B. S. V., & Mishra D. C. (2001) Density inhomogeneities under
576 Deccan Volcanic Province as derived from gravity data. *Journal of Geodynamics,*
577 *31*(1), 1-17. https://doi.org/10.1016/S0264-3707(00)00015-6

578 Ward, K. M., Zandt, G., Beck, S. L., Christensen, D. H., & McFarlin, H. (2014). Seismic
579 imaging of the magmatic underpinnings beneath the Altiplano-Puna volcanic complex
580 from the joint inversion of surface wave dispersion and receiver functions. *Earth and*
581 *Planetary Science Letters*, *404*, 43-53. https://doi.org/10.1016/j.epsl.2014.07.022

582 Watanabe, T. (1993). Effects of water and melt on seismic velocities and their application to
583 characterization of seismic reflectors. *Geophysical Research Letters*, *20*(24), 2933-
584 2936. https://doi.org/10.1029/93GL03170

585 Zhai, Y., & Levander, A. (2011). Receiver function imaging in strongly laterally
586 heterogeneous crust: Synthetic modeling of BOLIVAR data. *Earthquake Science*,
587 *24*(1), 45-54. https://doi.org/10.1007/s11589-011-0768-4

588 Zheng, T. Y., He, Y. M., Yang, J. H., & Zhao, L. (2015). Seismological constraints on the
589 crustal structures generated by continental rejuvenation in northeastern China.
590 *Scientific Reports*, *5*(1), 1-8. https://doi.org/10.1038/srep14995

591 Zinke, J. C., & Zoback, M. D. (2000). Structure-related and stress-induced shear-wave
592 velocity anisotropy: observations from microearthquakes near the Calaveras Fault in
593 Central California. *Bulletin of the Seismological Society of America*, *90*(5), 1305-
594 1312. https://doi.org/10.1785/0119990099

595 Zhu, L., & Kanamori, H. (2000). Moho depth variation in southern California from
596 teleseismic receiver functions. *Journal of Geophysical Research: Solid Earth,*
597 *105*(B2), 2969-2980. https://doi.org/10.1029/1999JB900322

598 Zorin, Y. A., Turutanov, E. K., Mordvinova, V. V., Kozhevnikov, V. M., Yanovskaya, T. B.,
599 & Treussov, A. V. (2003). The Baikal rift zone: the effect of mantle plumes on older
600 structure. *Tectonophysics*, *371*(1-4), 153-173. https://doi.org/10.1016/S0040-
601 1951(03)00214-2